Ice-Assisted Cryogenic Embrittlement Grinding for Surfactant-Free Fabrication of Soft Nanomaterials

Yangjie Fu[a, b, †], Xunan Wei[b, c, †], Tianyu Wang[d, †], Yi Peng[a], Shuwang Wu[e], Ke Li[d, *], Dongsheng Liu[f], Jianjun Wang[g, h, *], Yuanchen Dong[b, c, *], Jie Liu[a, b, *]

[a] Beijing National Laboratory for Molecular Science, CAS Key Laboratory of Green Printing, Institute of Chemistry, Chinese Academy of Sciences, Beijing 100190, P. R. China

[b] School of Chemical Sciences, University of Chinese Academy of Sciences, Beijing 100049, P. R. China.

[c] Beijing National Laboratory for Molecular Science, CAS Key Laboratory of Colloid, Interface and Chemical Thermodynamics, Institute of Chemistry, Chinese Academy of Sciences, Beijing 100190, P. R. China.

[d] Department of Plastic and Burn Surgery, The First Affiliated Hospital of Soochow University, Suzhou 215123, P. R. China.

[e] State Key Laboratory of Radiation Medicine and Protection, School of Radiation Medicine and Protection, Soochow University, Suzhou 215123, P. R. China.

[f] Department of Applied Biology and Chemical Technology, The Hong Kong Polytechnic University, Hong Kong 999077, P. R. China.

[g] Technical Institute of Physics and Chemistry, Chinese Academy of Sciences, Beijing 100190, P. R. China.

[h] School of Future Technology, University of Chinese Academy of Sciences, Beijing 100049, P. R. China.

[†] These authors contributed equally to this work.

Table of Contents

Experimental Section

Cell culture

Hela cells and HepG2 cells were individually cultured in medium. All culture media were supplemented with 10% FBS (GIBCO, Thermo-fisher scientific) and 1% penicillin-streptomycin (GIBCO, Thermo-fisher scientific). Cells were continuously cultured in an incubator with saturated humidity (37 ℃ and 5% CO_2). When cells grew to ubconfluence (75-85%). DMEM media were removed and the cells were washed once with PBS (pH =7.2) and treated with 0.25% trypsin. The digesting cells were counted by cell counter (thermo-fisher scientific).

Confocal laser scanning microcopy (CLSM) imaging

Hela cells at a density of were seeded in confocal plates and incubated for 24 h. The cells were incubated with medium including Cy5-Nanogels for 4 h and then rinsed three times with phosphate buffered saline (PBS, pH = 7.2). Subsequently, the cells were stained with Hoechst 33342 Staining Dye Solution for 15 min at 37 ℃ before imaging with confocal laser scanning microscope (Leica) with excitation.

The MTS assay

Hela cells were placed in 96-well plates with a density of 10000 mL^{-1} (100 μL/well) in DMEM media and cultured for 24 h. After incubation period, the medium was removed, followed by adding fresh DMEM medium including 10 μL ASO-Nanogel or Paclitaxel-Nanogel. The cells were then cultured in DMEM medium with different ASO-Nanogel or Paclitaxel-Nanogel for further 24 h, 48 h and 72 h. And then, cell viability was measured by using the standard MTS [3-(4,5-dimethylthiazol-2-yl)-5-(3-carboxymethoxyphenyl)-2-(4-sulfophenyl)–2H-tetrazolium] assay via CellTiter 96® Aqueous One Solution Cell Proliferation Assay Kit. For Hela cell growth experiment, untreated Hela cells were measured for 24 h, 48 h and 72 h. The optical density of each well was measured at a wavelength of 490 nm on a microplate reader (E-max, Molecular Devices, Sunnyvale, CA). Calculate the corresponding number of cells according to the optical density.

The characterization of PCSK-9 mRNA level

The gene expression of PCSK-9 was assessed using RT-qPCR analysis. The total RNA was extracted from differently treated cells incubated for 24 h with FastPure Cell/Tissue Total RNAIsolation Kit V2 (Vazyme). RT-qPCR was conducted 40 cycles at 95 ℃ for 15 s and at 60 ℃for 60 s using an Archimed RT-qPCR instrument. All experiments were triplicated and analyzed by $2^{-\triangle\triangle Ct}$ method, with GAPDH gene as an internal standard. More about $2^{-\triangle\triangle Ct}$ method can refer to another protocol published. Here, Ct in the formula is abbreviated for cycle threshold. Data were reported as a mean ± standard deviation. Values were compared in GraphPad Prism using a two tailed unpaired t-test or ANOVA.

Antibacterial Characterization of powders

E. coli (ATCC8739, gramnegative bacteria) and *S. aureus* (ATCC 6538, a gram-positive bacteria) were selected as test strains to evaluate the antibacterial activity of the powders. 100 μL of *E. coli* or *S. aureus* solution with the concentration of 10^7 CFU mL^{-1} was dropped onto the samples, and incubated at 37℃ for 2 h. Then 900 μL of PBS was added and mixed

thoroughly. Subsequently, 10 μL of solution was taken out, evenly spread on the pre-prepared agar plate, and incubated at 37℃ for 18 h. Finally, the number of bacterial colonies on the agar plate was counted. Similarly, 100 μL of *E. coli* or *S. aureus* solution at the concentration of 10^7 CFU mL^{-1} was co-incubated with the sample for 2 h, followed by the addition of 900 μL of Luria–Bertani (LB) broth to submerge the sample, and further incubated at 37°C for 18 h.

Antioxidant activity of samples

The antibacterial activity of DP@TCP-gel was examined via ABTS and DPPH methods. First, the antioxidant capacity of TA was evaluated. Equal volumes of ABTS (7.4 mM) and potassium persulfate (2.6 mM) were mixed and allowed to react for 16 hours at 4 °C in the dark to prepare the ABTS+ free radicals. Subsequently, 200 μL of sample solution (20 μg mL^{-1}) was mixed with 600 μL of ABTS+ radicals. After 6 minutes, the UV absorption spectrum was scanned from 450 nm to 950 nm, and the absorbance at 734 nm was measured. The ABTS+ scavenging activity was calculated according to the following: ABTS+ scavenging (%) = $(A_0 - A_t)/ A_0 \times 100\%$, where A_0 represented the absorbance of pure ABTS, and At represented the absorbance of ABTS+ free radicals with treatment.

As for the scavenging of DPPH• free radicals, DPPH reagent (100 μM) was first dissolved in ethanol to prepare the DPPH• free radicals. Subsequently, 50 μL of sample solution at different concentrations was added to 950 μL of DPPH• free radicals (50 μL of PBS as the negative control). The mixture was then incubated in the dark for 30 minutes. After incubation, the absorbance was scanned from 450 nm to 600 nm, and the absorbance at 517 nm was used to calculate the DPPH• scavenging rate as the following equation: DPPH• scavenging (%) = $(A_{negative} – A_{sample})/ (A_{negative} – A_{blank}) \times 100\%$, where $A_{negative}$ represented the absorbance of the mixture of 950 μL DPPH• radicals and 50 μL PBS, A_{sample} represented the absorbance of the sample treated group, and A_{blank} was the absorbance of the PBS solution without DPPH• radicals.

Whole Blood Clotting Index Test

To initiate clotting, 0.1 M $CaCl_2$ solution (10% v/v) was added to whole pig blood and mixed by vortexing. 100 μL of recalcified whole blood solution was added to 5 mg of powder. After incubation at 37℃ with shaking (100 rpm) for 5 min, unstable blood clots were dissolved by adding 5 mL of deionized water. The hemoglobin content of the supernatant was measured at 540 nm using a microscopic spectrophotometer. The blood clotting index (BCI) was calculated as BCI (%) = $(I_s – I_0)/(_{Ic} – I_0) \times 100\%$, where I_s represented the absorbance value of the sample, I_c represented the absorbance value of the positive control group where 5 mL of deionized water was directly dropped into 100 μL of recalcified blood, and I_0 represented the absorbance value of the blank plate.

In Vitro Blood Clotting Time Test

To initiate clotting, 0.1 M $CaCl_2$ solution (10% v/v) was added to citrated blood and mixed by vortexing. Then, 5 mg of each powder samples was placed in 2 mL centrifuge tube each containing 100 μL of the calcium-treated blood. At specific time points, each centrifuge tube

was rinsed with 400 μL PBS. The clotting time was defined as the point at which a uniform, stable clot remained after washing.

In Vivo Wound Healing Assessments

Animal experiments of this study were performed in accordance with the protocols approved by the Animal Ethics Committee of Soochow University (approval number: 202510A0696). Male C57BL/6 mice (6–8 weeks old) were used in this study and were purchased from Changzhou Cavens Laboratory Animal Co., Ltd. The mice were housed in a pathogen-free environment with controlled temperature and humidity, and they had free access to food and water. After a one-week acclimation period, the mice were randomly divided into three groups (n = 3 per group): a blank control group, a nanogel group, and a nanogel-drug group. A full-thickness skin excision wound with a diameter of 8 mm was created on the dorsal region of each mouse.

During each treatment, 20 mg of the prepared nanogel or nanogel-drug powder was evenly applied to the wound surface in the experimental groups, followed by the addition of 100 μL of normal saline. In contrast, the control group received only 100 μL of normal saline. After 10 min, all wounds were covered with sterile gauze. Dressings were changed every two days, and wound images were recorded on days 0, 3, 5, 7, and 14 after treatment. The wound area was quantified using ImageJ software, and all measurements were normalized to a scale bar.

Histological analysis

Histological analysis of wound healing was performed 14 days post-treatment using hematoxylin and eosin (H&E) and Masson's trichrome staining. On day 14, all mice were euthanized, and skin tissues from the wound sites were excised. Nine skin samples were fixed in 4% paraformaldehyde for 48 hours, embedded in paraffin, and sectioned for H&E and Masson staining. Histological and fluorescence images were acquired using CaseViewer, and scale bars were added using ImageJ software.

Statistics analysis

Statistical analysis and figure generation were performed using GraphPad Prism. All data are presented as mean±standard deviation. Comparisons were conducted using one-way ANOVA and Tukey's posthoc test. Statistical significance was defined as $^{*}P < 0.05$, $^{**}P < 0.01$, and $^{***}P < 0.001$.

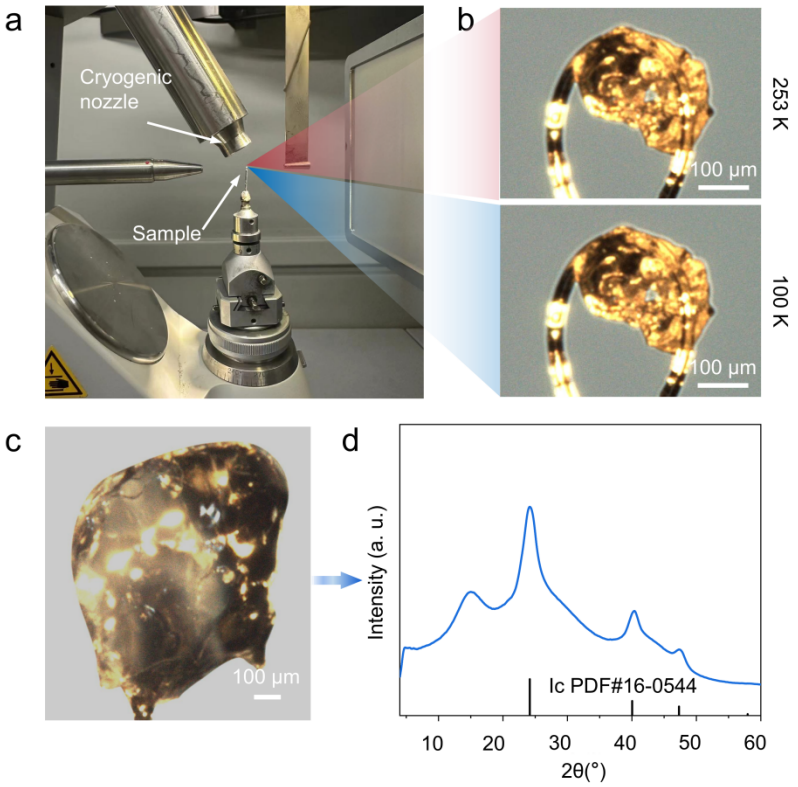

Supplementary Figure 1. In-situ variable temperature X-ray diffraction (XRD) characterization of PAG macrogel. **a,** Experimental setup for in-situ variable-temperature single-crystal X-ray diffraction. The macrogel sample is mounted on a copper loop, with temperature precisely controlled by a continuous stream of chilled nitrogen from the nozzle. **b,** Digital photographs of the gel sample captured at 100 K and 253 K during temperature cycling. No observable structural changes occur across this temperature range. **c,** The photos of macrogel with the cubic millimeter size at 100 K. **d,** The XRD spectrum shows the diffraction crystallization peaks of macrogel during the in-situ quenching. According to standard card (PDF#16-0544), these peaks correspond to crystallization peaks of cubic ice (I_c), suggesting the growth of crystalline ice in the macrogel. It is caused by the uneven temperature in the gel, which may damage the gel network structure and impair the subsequent fragmentation uniformity. Therefore, it is necessary to reduce the volume of hydrogel before quenching treatment.

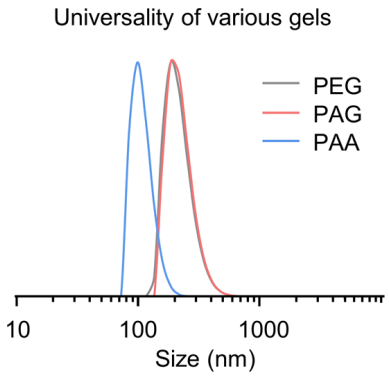

Supplementary Figure 2. Universality experiment. DLS spectra demonstrate the size distributions of different nanogels in water. The additive used is NaCl. The ratio of hydrogel and additive is 1:1. Grinding cycle is 7 cycles. Following 7 grinding cycles, the resulting sizes of PEG, PAG and PAA nanogels exhibit approximately diameters of 108 nm, 110 nm and 94 nm, respectively.

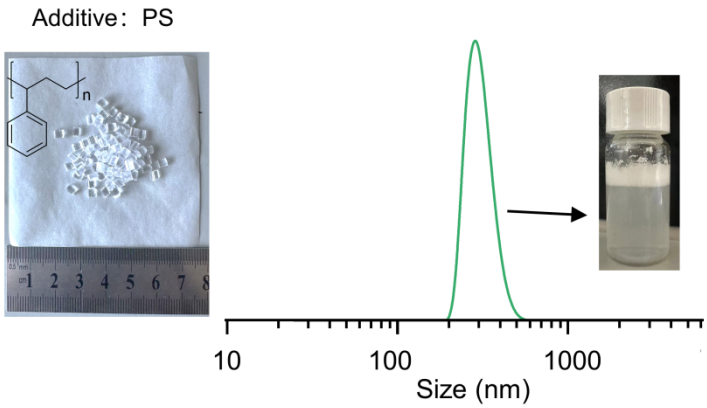

Supplementary Figure 3. The size and dispersion state of nanogels in water after fragmentation with insoluble additives. DLS spectrum presents the size distribution of nanogels when fabricated with polystyrene (PS) particles. The left insert photo shows original PS particles. The right insert photo shows that the water-soluble nanogels well-dispersed in water, while the hydrophobic PS particles separate and float to the surface.

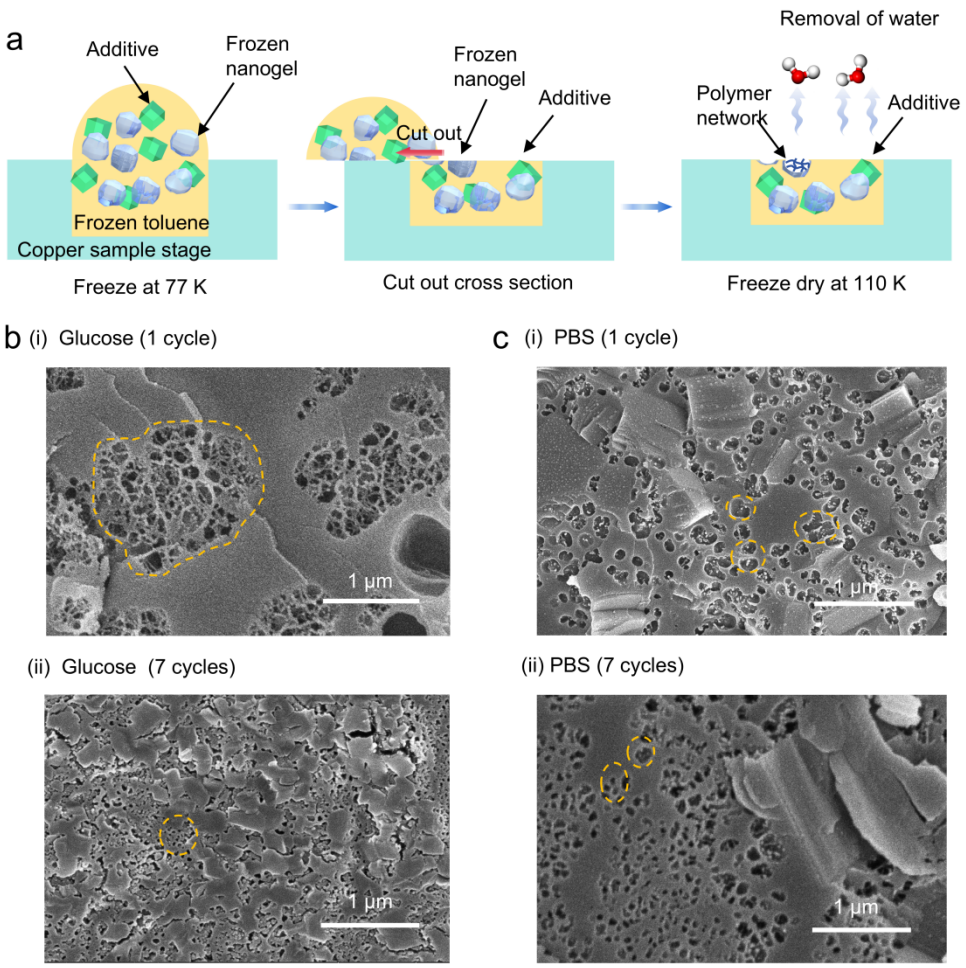

Supplementary Figure 4. The morphology of various additives and PAG nanogels. **a**, Schematics illustrate the protocol for preparing samples for Cryo-SEM. The obtained powder mixture was dispersed in toluene and frozen in liquid nitrogen, followed by an in-situ section and freeze-drying procedure at 110 K to selectively dehydrate nanogels at the cross section. **b**, **c**, Cryo-SEM images illustrate the size and morphology of the PAG nanogels and various addtives after fragmentation for different cycle numbers: glucose powder for 1 cycle and 7 cycles (**b**), PBS powder for 1 cycle and 7 cycles (**c**). As cycles increase, nanogel size reduces to below 100 nm for both glucose or PBS.

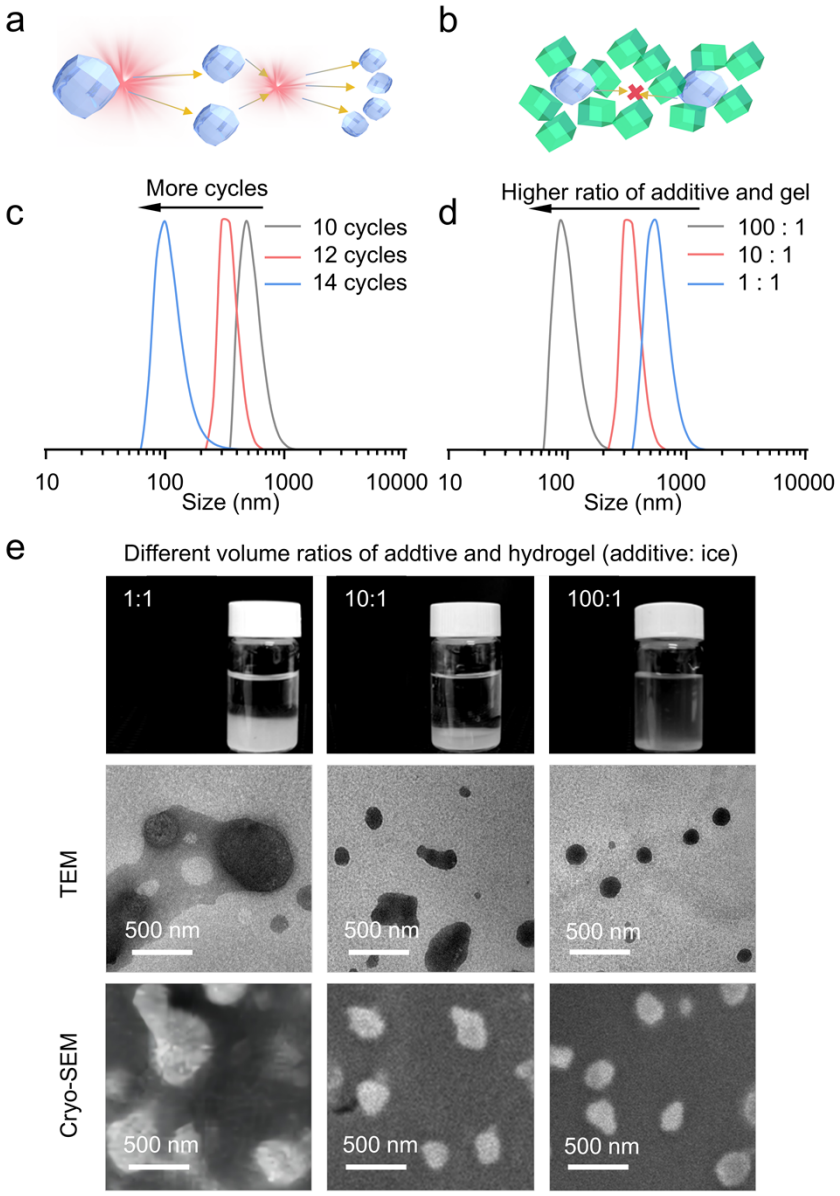

Supplementary Figure 5. Comparison of PEG nanogels after grinding with ice under different conditions. **a, b,** Schematics show the progressive fragmentation of the frozen gel over time (**a**), and additive induces spacing effect, hindering gel re-aggregation (**b**). **c, d,** DLS spectra of PEG nanogels after fragmentation with varying cycle numbers (**c**) and ratios of additives and hydrogel (**d**). The additive used is ice. With the increase of the cycle numbers, the size of the nanogel decreased from about 640 nm to 100 nm, suggesting prolonged processing time enables further size reduction. **e,** The influence of the different volume ratios of hydrogel and additive on the resulting nanogel size. Grinding cycle is 10 cycles. Digital photos show the nanogel dispersion in aqueous solutions. The TEM and Cryo-SEM images show the morphology of PEG nanogels after fragmentation with different ratios of additives and hydrogel. Grinding cycle is 10 cycles. With the ratio of ice and gel increases from 1:1 to 100:1, visible size decreases and shape becomes more regular, highlighting ice's role in separating gel particles.

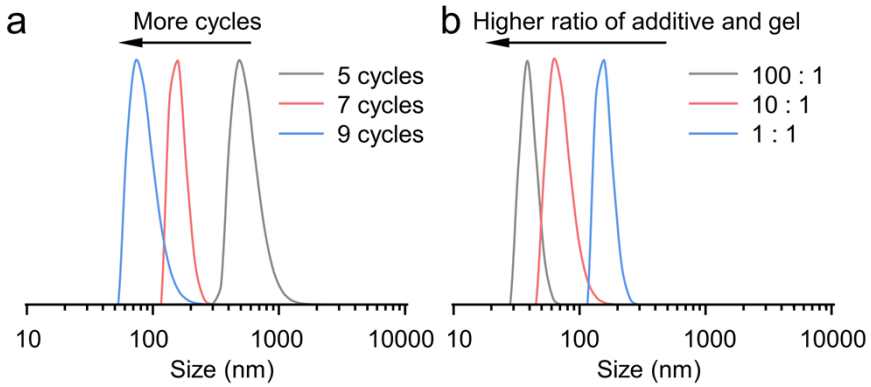

Supplementary Figure 6. Comparison of PEG nanogels after grinding with NaCl under different conditions. **a,** DLS spectra demonstrate the size distributions of PEG nanogels in water with varying cycle numbers. The ratio of hydrogel and additive is 1:1. With the increase of the cycle numbers, the size of the nanogel decreases from about 108 nm to 70 nm, indicating extended processing time enables further size reduction and more additive choices. **b,** The influence of the different volume ratios of hydrogel and additive on the resulting nanogel size. Grinding cycle is 7 cycles. Similar to the result of ice as additive, extending running time and reducing particle size is a universal trend. As the ratio of NaCl and gel increases from 1:1 to 100:1, the visible size decreases from about 108 nm to 40 nm, proving lower size limit accessibility.

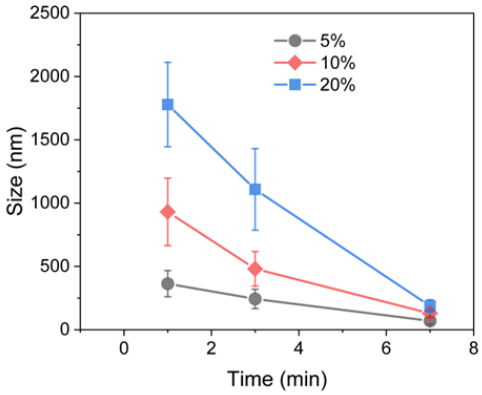

Supplementary Figure 7. Evolution of nanogel size derived from PAG hydrogels of varying solid contents as a function of grinding cycle number.

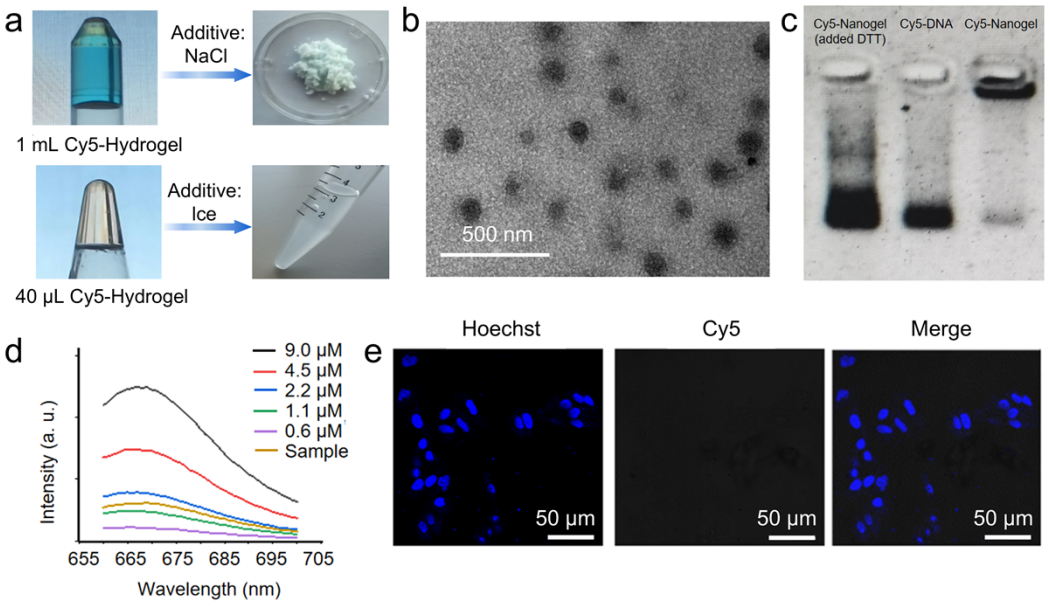

Supplementary Figure 8. Characterization of nanogel for drug delivery. **a,** The state of PEG gels loaded with Cy5-DNA after cryo-solidified fragmentation with additives. The additive used is NaCl or ice. **b,** The morphology of Cy5-Nanogel under TEM. **c,** Electrophoretic analysis (10% PAG) of Cy5-Nanogel. **d,** Fluorescence spectrum of Cy5-Nanogel and Cy5-DNA solution with different concentrations. **e,** Laser scanning confocal microscopic images of the Hela cells.

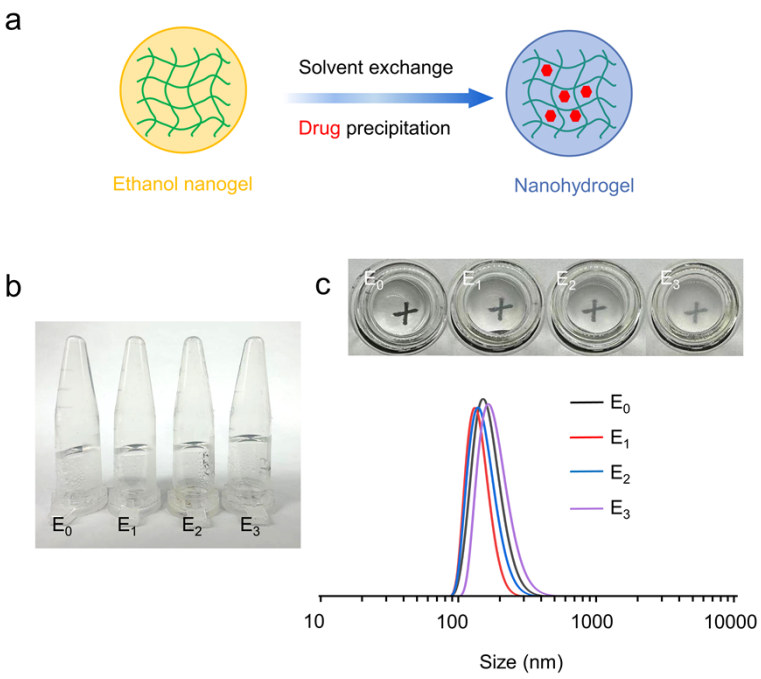

Supplementary Figure 9. High drug loading of PTX by nanoalcogel. **a**, Schematic illustration of the formation of high PTX loading nanogel via solvent exchange. **b**, Digital photos of ethanol gel with different drug loading of PTX. E_0: 0 mg/mL, E_1: 5 mg/mL, E_2: 20 mg/mL, E_3: 60 mg/mL. **c,** DLS spectra present the size distributions of high drug loading nanogels in water after cryo-solidified fragmentation. The additive used is NaCl. Grinding cycle: 7 cycles. The ratio of additive and hydrogel is 1:1. Digital photos show nanogel dispersed in aqueous solutions, with hydrophobic PTX locked in the gel via water - alcohol substitution.

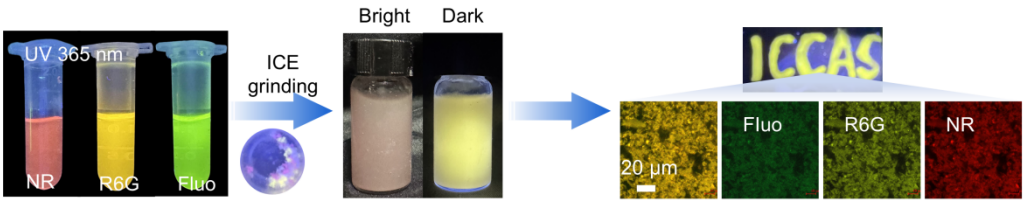

Supplementary Figure 10. Multi-nanogel for loading of diverse cargos. A multi-nanogel system encapsulating different fluorescent dyes (fluorescein (Fluo), rhodamine 6G (R6G), neutral red (NR)) prepared by ICE-grinding (left). Representative photograph and CLSM images of the multi-nanogel system (right).

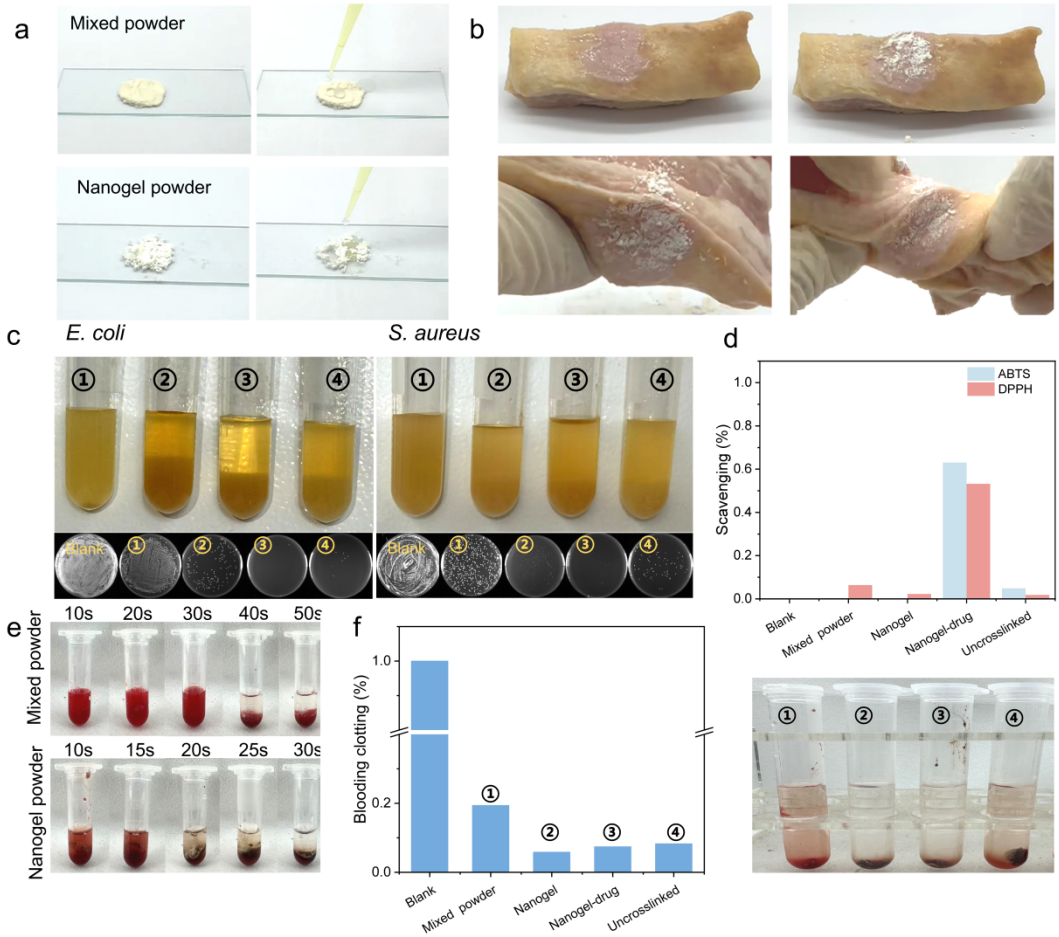

Supplementary Figure 11. In vitro properties of the nanogel dressing powder. **a,** Photographs showing rapid liquid absorption by the nanogel powder compared with a physical mixture of the component drugs. **b,** The nanogel powder absorbed interfacial moisture and formed a strong bond with porcine skin. **c,** Photographs of *E. coli* and *S. aureus* suspensions after co-culture with the indicated samples in nutrient broth. Insets show representative colony images obtained after 2 h co-culture, followed by plating on agar and incubation for 18 h. Groups: ① CS/Alg mixed powder; ② nanogel powder; ③ drug-loaded nanogel powder; ④ uncrosslinked nanogel powder. **d,** Antioxidant activity of sample extracts at different concentrations, evaluated by ABTS and DPPH assays. **e,** Photographs of blood clotting after adding nanogel powder to whole porcine blood. **f,** Blood clotting index (BCI) of the nanogel powder and control groups. Insets show photographs of samples incubated at 37 °C for 5 min, followed by addition of 5 mL deionized water.

As a powder wound dressing, the multifunctional performance of the nanogel powder was evaluated in vitro. Liquid absorption was assessed using a physical mixture of sodium alginate and chitosan powders as a control. Compared with the mixed powder, the nanogel powder rapidly absorbed droplets deposited on the powder bed, likely due to its gel network and surface-exposed hydrophilic groups that enhance interfacial wettability (SI Appendix, Figure 11a). On moist porcine skin, the nanogel powder formed a hydrogel in situ and exhibited robust,

dynamic adhesion, resisting external perturbations, including vigorous twisting (SI Appendix, Figure 11b).

As shown in Figure 10c, all powder formulations inhibited bacterial growth, consistent with membrane disruption by cationic chitosan. The drug-loaded nanogel achieved near-complete inhibition, primarily due to the incorporated antibiotics (gentamicin and vancomycin). Because wound infection can induce inflammation and oxidative stress, resulting in elevated reactive oxygen species (ROS) that damage cells and delay healing, antioxidant activity was evaluated using ABTS and DPPH assays. While the nanogel matrix showed minimal intrinsic antioxidant activity, encapsulated hydrophobic curcumin conferred strong antioxidant capacity (SI Appendix, Figure 11d).

Severe burns are frequently associated with significant blood loss, making rapid hemostasis essential. As shown in Figure 11e (SI Appendix), the nanogel powder triggered formation of a stable thrombus in reactivated anticoagulated whole blood within 25 s, markedly faster than the control. After 5 min co-incubation with reactivated anticoagulated whole blood, the blood clotting index (BCI) of the nanogel powder was 5.9%, substantially lower than that of the mixed-powder group (19.4%) (SI Appendix, Figure 11f). Notably, hemostatic performance was largely retained after loading multiple drugs (BCI = 7.4%). Collectively, the drug-loaded nanogel powder provides multifunctional therapeutic benefits, supporting its potential as a powder dressing for burn wound management.

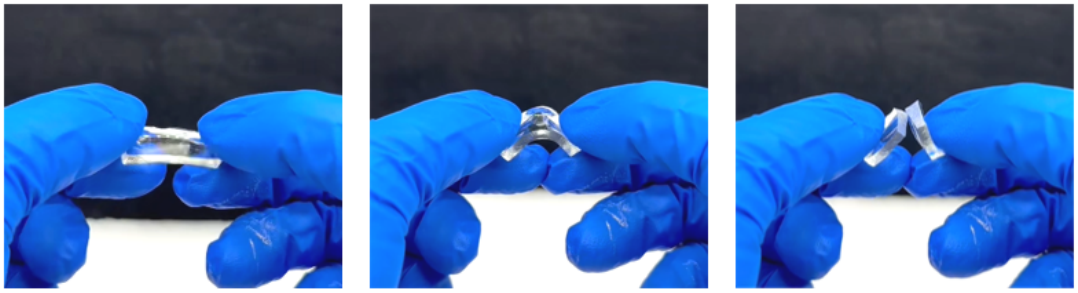

Supplementary Figure 12. Brittle fracture of PAG bulk hydrogel upon bending. The brittleness of bulk hydrogels compromises their conformability to irregular tissue surfaces.

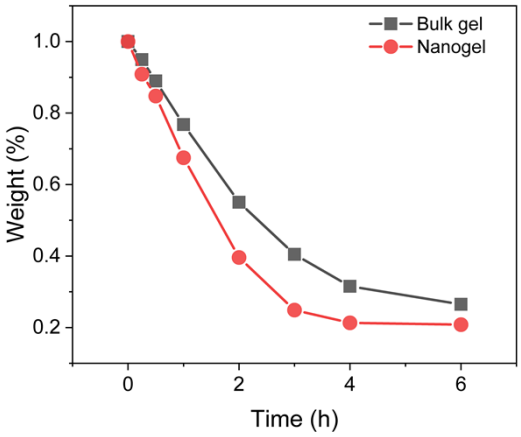

Supplementary Figure 13. Weight loss of bulk gel and nanogel as a function of time due to dehydration under ambient conditions. Compared to bulk hydrogels, nanogels exhibited accelerated water loss during the initial 4 h, followed by mass stabilization thereafter, presumably attributable to enhanced retention of residual moisture within the nanoscale gel network.

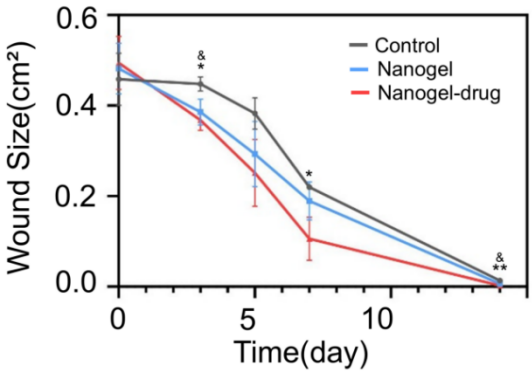

Supplementary Figure 14. Wound areas of each group at different post-treatment time points. Quantification of wound areas in the different treatment groups over the healing period. On day 3 and day 14, both nanogel-treated groups exhibited a statistically significant acceleration in wound closure relative to the control. Statistics: Data are presented as mean ± SD (n = 3). *p < 0.05, **p < 0.01 (Nanogel-drug vs. Control); &p < 0.05 (Nanogel vs. Control).

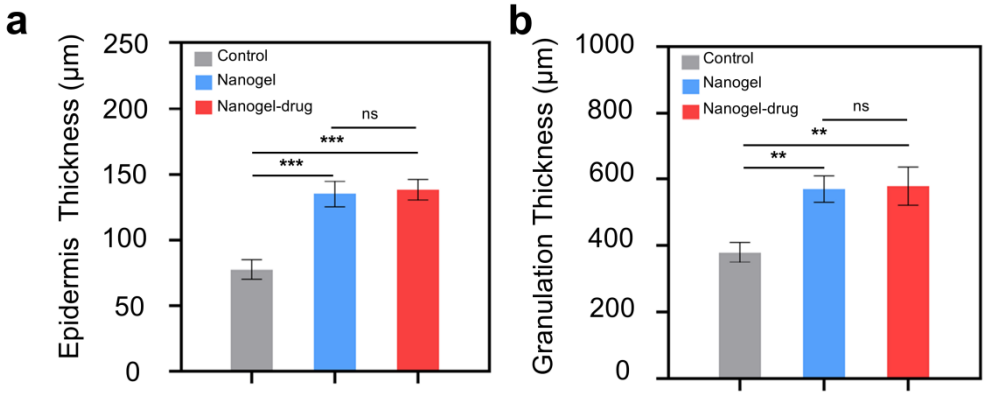

Supplementary Figure 15. Quantitative analysis of epidermal and granulation tissue formation in the different treatment groups over the healing period. a, Epidermis thickness of wound on day 14 (n = 3). b, Granulation tissue thickness of wound on day 14 (n = 3). After the wounds were treated by nanogel or nanogel-drug, the thickness of both epidermis and granulation tissue were significantly increased, providing them accelerated re-epithelialization compared to the control group.

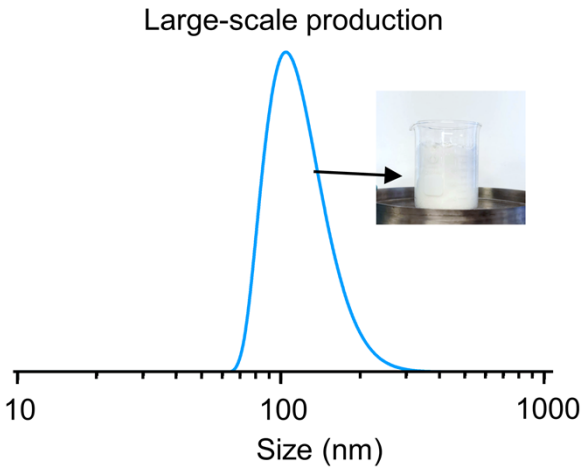

Supplementary Figure 16. Scalability experiment. DLS spectrum of PAG nanogels for large-scale (500 g) production. The additive used is NaCl. The ratio of additive and hydrogel is 1:1. Grinding cycle is 7 cycles.

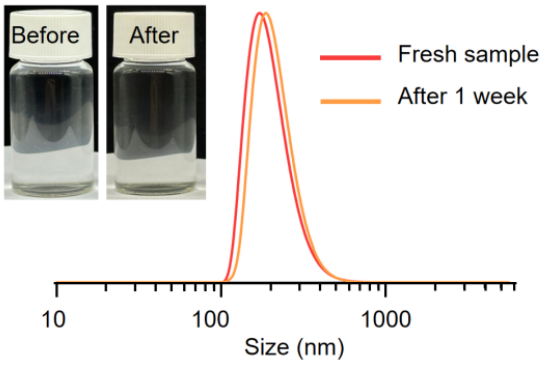

Supplementary Figure 17. The stability of PAG nanogels for long-term storage. DLS size distributions of PAG nanogels before (left)/after (right) after one week of static storage. Insets, photographs of the corresponding aqueous dispersions, illustrating differences in colloidal stability. The additive used is NaCl. The ratio of additive and hydrogel is 1:1. Grinding cycle is 7 cycles.

Supplementary Table 1. DNA sequences

	Sequence 5'-3'
Cy5-DNA	Cy5-TTTATGGCGCACGCTG-SH
Bcl2-ASO	SH-TCTCCCAGCGTGCGCCAT
Sense PCSK-9	CUAGACCUGUUUUGCUUUUGU-SH
Antisense PCSK-9	ACAAAAGCAAAACAGGUCUAGAA
Sense GAPDH	GGAGCGAGATCCCTCCAAAAT
Antisense GAPDH	GGCTGTTGTCATACTTCTCATGG

Supplementary Table 2. Statistical information for Figure 3g.

Figure number	Figure 3g
Independent sample size	n = 3
Cell line	Hela cells
Data presentation	mean ± SD
Added drugs	PBS
	Nanogel
	ASO-Nanogel
Statistical test	Cell viability
Monitor time	24 h, 48 h, 72 h

Supplementary Table 3. Statistical information for Figure 3h.

Figure number	Figure 3h
Independent sample size	n = 3
Cell line	HepG2 cells
Data presentation	mean ± SD
Added drugs	PBS
	Nanogel
	siRNA-Nanogel
	SiRNA-lipo3000
Statistical test	Relative PCSK9 mRNA level
Monitor time	24 h, 48 h, 72 h

Supplementary Table 4. Statistical information for Figure 3i.

Figure number	Figure 3i
Independent sample size	n = 3
Cell line	Hela cells
Data presentation	mean ± SD
Added drugs	PBS
	Nanogel
	Paclitaxel-Nanogel
Statistical test	Cell viability
Monitor time	24 h, 48 h, 72 h